Molecular Analysis of Selective Gas Adsorption within Composites of Ionic Polyimides and Ionic Liquids as Gas Separation Membranes

Asghar Abedini, Ellis Crabtree, Jason E. Bara, and C. Heath Turner*

Department of Chemical and Biological Engineering, The University of Alabama,

Box 870203, Tuscaloosa, Alabama 35487, USA

*Corresponding author: hturner@eng.ua.edu
(205) 348-1733 (phone)
(205) 348-7558 (fax)

Abstract

The CO_2 separation characteristics of ionic polyimides (i-PIs) are modeled using molecular dynamics simulations in combination with grand canonical Monte Carlo calculations. The performance of neat i-PI systems is evaluated, as well as composite structures containing both i-PIs and various ionic liquids (ILs). The i-PI+IL composites are based on combinations of 1-*n*-butyl-3-methylimidazolium ($[C_4mim^+]$) cations with three common molecular anions: (bis(trifluoromethylsulfonyl)imide ($[Tf_2N^-]$), tetrafluoroborate ($[BF_4^-]$), and hexafluorophosphate ($[PF_6^-]$). It is found that 50 mol% IL inclusion can increase CO_2/CH_4 selectivity by 16% in $[BF_4^-]$-based materials and by 36% in $[PF_6^-]$-based materials from mixtures of 5% CO_2 / 95% CH_4. While the $[BF_4^-]$-based system shows higher CO_2/CH_4 selectivity, the $[Tf_2N^-]$-based system shows higher CO_2/N_2 gas selectivity. A comprehensive structural analysis (fractional free volume (FFV), pore size distribution, surface area, etc.) is used to highlight the underlying differences among the different i-PI+IL systems that lead to the different adsorption properties.

Keywords

Porosity; molecular dynamics; Monte Carlo; selectivity; imidazole; polymer

1. Introduction

Carbon dioxide (CO_2) is the most well-known greenhouse gas (GHG) with many industrial emission sources contributing to the detriment of the atmosphere. CO_2 removal from natural gas has been successfully applied for over 80 years.[1] Although amine-based solvents, such as monoethanolamine (MEA) exhibit multiple disadvantages including corrosion, volatility, toxicity, and high-energy demand for recovery, carbon capture processes still heavily depend on typical MEA solvents during CO_2 absorption due to the high cost or low efficiency of other alternatives.[2] The design of alternative materials for CO_2 capture is of high importance due to a growing need for control of CO_2 emissions to the atmosphere and for increasing the efficiency of energy supply lines by reducing CO_2 in pre-combustion gases. Several different adsorbents such as activated carbons,[3] zeolites,[4] metal organic frameworks (MOFs),[5] and covalent organic frameworks (COFs)[6] have been widely studied for CO_2 adsorption. These materials provide a high capacity for gas adsorption, but they typically suffer from other limitations (selectivity, cost, or stability).

In addition to these porous materials, different types of ionic liquid (IL) solvents have also been studied and proposed as effective alternatives for CO_2 absorption.[7] These IL solvents have previously been shown to be effective at dissolving CO_2, and they tend to possess high thermal and physical stability and low vapor pressure. In particular, imidazolium-based ILs have received a great deal of attention, due to their high solubility and selectivity for CO_2 in post-combustion capture and natural gas sweetening.[8-14] However, their high cost and high viscosity as well as their limited adsorption capacity for CO_2 render them to be uncompetitive with traditional gas absorbents used in industrial-scale applications.[8,9]

There have been some previous efforts to circumvent the inherent IL performance limitations. For instance, dissolving ILs in an amorphous structure of polymers and crystal structures consisting of MOFs[11] and COFs[15] can alleviate the low capacity of ILs by providing more void volume.[14] Recently, to explore the directed orientation of IL molecules and the resulting effect on gas separation, others have investigated the properties of ILs confined within solid pores.[5,8,14,16-18] In those works, a thick layer of IL solvent was confined between solid surfaces,[19] and gas diffusion in that confined layer was studied, as well as the influence of confinement on CO_2 solubility.[14,20,21] Budhathoki, et al. used molecular dynamics (MD) simulations to study CO_2 solubility selectivity, diffusion selectivity, and permselectivity from binary mixtures of CO_2/CH_4 and CO_2/H_2 within a [C_4mim][Tf_2N] confined IL solvent.[8] The IL was confined within graphite nanopores of 2 to 5 nm in diameter. The ILs confined within the pores demonstrated enhanced permselectivity of CO_2 (compared to the empty nanopores), but the diffusivity of all gas species decreased, relative to bulk ILs. Expelling captured CO_2 during adsorption and absorption and recycling the adsorbent and absorbent liquids is already a cost effective process in separation columns. However, membrane separation mitigates the need for frequent adsorbent replacement and absorbent recovery by providing continuous gas separation and purification.[22-24]

Porous organic polymers[25-27] have been considered in gas separation studies due to their stability,[28,29] large surface area,[30,31] and fine-tuned microporosity resulting from the voids created in their rigid molecular structure (due to frustrated polymer chain packing).[32-35] Supported ionic liquid membranes (SILMs)[36] and polymers of intrinsic microporosity (PIMs)[23,37] are now receiving much attention due to the combined advantages of both ILs

and membranes in gas separation.[24,38-41] For instance, CO_2 mass transfer can be significantly enhanced when ILs are dissolved into polymers and porous solid structures.[5,42] Also, nitrogen-rich polymer building blocks can help promote CO_2 uptake within amorphous microporous polymers (AMPs) by increasing the heat of adsorption.[33,43]

Ionic polyimides (i-PIs) are one of these promising polymers for membrane-based CO_2 separations (pre-combustion, gas sweetening, and CO_2 post-combustion capture).[42,44] This novel class of materials, like poly(ionic liquids)s (PILs),[45,46] contain imidazolium cations within the polymer monomer unit. In the poly(ionic liquid) structure, IL molecules are bonded to the polymer backbone. However, the i-PI monomer structure is composed of an IL segment and an organic linker to provide an additional degree of structural and chemical design. In the i-PI structure, 1-(3-aminopropyl)imidazole is reacted with pyromellitic dianhydride (PMDA) to form a difunctional bis(imidazole) molecule which is then reacted with p-dichloroxylene to form the ionic polyimide. The chloride (Cl^-) anions resulting from the polymer synthesis (Menshutkin Reaction) are subsequently exchanged to bistriflimide (Tf_2N^-), hexafluorophosphate (PF_6^-) or tetrafluoroborate (BF_4^-) in the presence of aqueous solutions of the corresponding alkali metal salt in excess. PMDA was chosen as an organic ligand because of its low cost and reports that the PMDA-API molecule forms triply helical nanostructures in the presence of silver salts.[47] Each monomer contains two imidazolium cations in the backbone, along with two balancing anion molecules, as illustrated in Figure 1. Composite structures were prepared by dispersing IL molecules inside the i-PI polymer in different concentrations.

Our previous experimental work[42] reports the significantly enhanced CO_2 permeability (up to 2200%) by adding $[C_4mim][Tf_2N]$ to the neat i-PI system. The high permeability in

the composite system (i-PI + IL) was directly correlated with diffusivity enhancement of CO_2 (up to 2300%), while solubility of CO_2 in the material was essentially identical in the presence/absence of IL. In order to characterize the molecular-level behavior of different gas adsorbents (CO_2, CH_4, N_2) in this system, our previous work[44] focused on pure gas solubility in [Tf_2N^-]-based structures. However, due to the intriguing potential for creating different composites by combining different ILs with the same i-PI backbone, the current work explores the selective adsorption behavior of binary gas mixtures with a range of different i-PI + IL composite materials. For instance, adding bulkier anions may increase the void volume of the composite and specific interactions with different anions may be used to tune the selectivity. In bulk ILs, it has been found that the anions can have a large influence on CO_2 solubility.[9] In the current study, the prepared composite structures contain i-PIs and different ILs with [C_4mim^+] as the cation in combination with one of three anions [Tf_2N^-], [BF_4^-], and [PF_6^-]. MD calculations and grand canonical Monte Carlo (GCMC) simulations are used to study structural changes of the i-PIs and their composites during binary mixtures of CO_2/CH_4 and CO_2/N_2 adsorption by analyzing the fractional free volume (FFV), pore size distribution (PSD), and the surface area.

In our current study, the neat i-PI with [BF_4^-] as the counter ion shows high CO_2/CH_4 selectivity at 1 bar and 294 K, and this is also observed when additional [C_4mim][BF_4] is added to generate the composite material. A high CO_2 solubility is found with the [PF_6^-]-based i-PI and i-PI + IL composites. The high solubility is accompanied by a large calculated surface area within the materials and a larger fraction of wider pores, while the FFV is not a very sensitive indicator of the solubility. Among the three different types of

anions studied in this work, the [PF_6]-based structures showed the strongest interaction with gas molecules, regardless of gas type.

2. Simulation Details

Our simulation procedure is comprised of several different steps in order to generate the initial configurations, relax the system, perform gas adsorption, and analyze the dominant molecular-level interactions. First, quantum mechanical calculations are used to assign partial charges on the atom sites of the i-PI monomer units (Figure 1) using the B3LYP functional[48] and a 6-31G(d,p) basis set in Gaussian09.[49] Then MD simulations are used to prepare the relaxed initial structure of the neat i-PI and i-PI + IL composite. This involves a polymerization scheme followed by several stages of structural relaxation. The initial system also contains an N-methyl-2-pyrrolidone (NMP) solvent, which is eventually removed and replaced with the IL species following polymerization. This is intended to qualitatively follow the experimental synthesis procedure during the polymerization and prepare enough vacant space for IL molecules by deleting NMP molecules.[42] Finally, using an iterative combination of molecular dynamics and GCMC simulations, the selectivity of CO_2/CH_4 and CO_2/N_2 is modeled over a wide range of concentrations within the neat i-PI and different combinations of i-PI + IL composite materials. The details of each stage are described below, which follows our previous approach.[44]

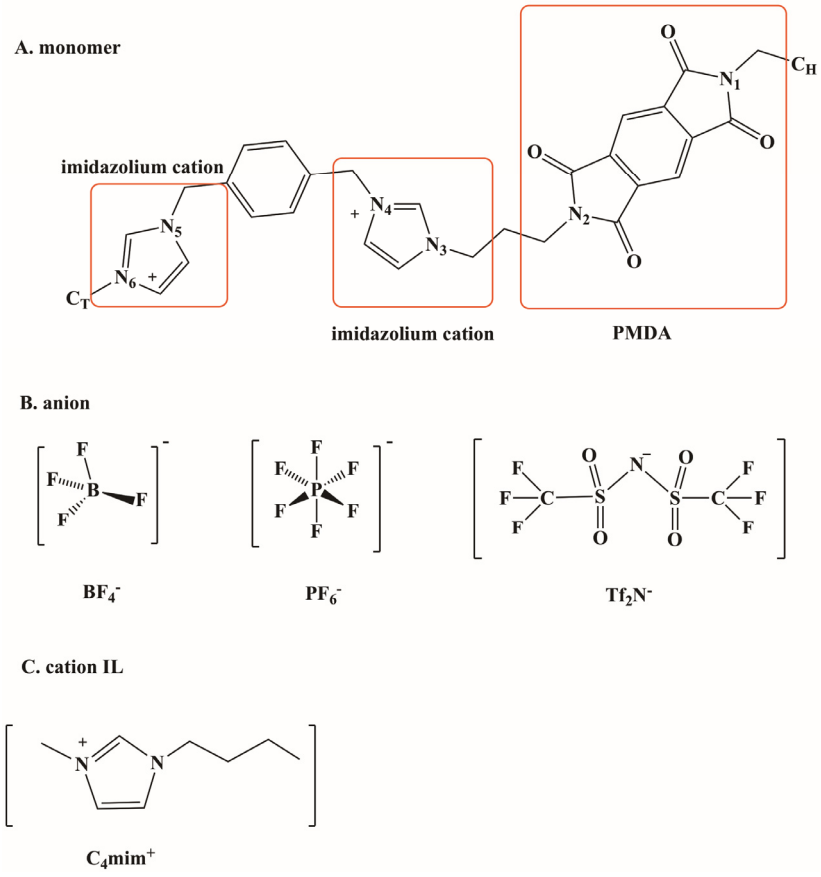

Figure 1. Representative monomer structure of a neat i-PI. Specific nitrogen sites of the i-PI are labeled for reference, as well as the head (C_H) and tail (C_T) designation.

The details of the electronic structure calculations and geometric optimization of the monomers, as well as the partial charge calculation and polymerization were provide in our previous work.[44] Force field parameters for [C_4mim^+], [Tf_2N^-], [BF_4^-], and [PF_6^-] were taken from Lopez, et al,[50-52] while parameters for NMP molecules were extracted from Aparicio, et al.[53] The TraPPE[54] force fields for CO_2, CH_4, and N_2 were used, based on the previous experience of others modeling gas adsorption in ILs.[54-57] The Lorentz-Berthelot mixing rules were used for cross-term interactions.

Following the assignment of the force fields, the i-PI and i-PI + IL systems were constructed and conditioned according to the following default procedure (with specific variations noted later in the text):

a) i-PI molecules (as single repeat units) were inserted into the simulation box using PACKMOL,[58] followed by energy minimization using the steepest descent algorithm.[59]

b) In addition to the monomers, NMP molecules were also inserted at three different ratios: 1:4, 1:6, and 1:8 (monomer:NMP) in order to produce additional replicas of the polymer structure. The experiments used a ratio of approximately 1:60 during polymerization.[42] The effect of different NMP solvent concentrations has been studied in our previous work,[44] and it was found to be negligible. We have reached the same conclusion in this work (with different ILs).

c) The monomer + NMP molecules were relaxed with MD simulations using a cycle of canonical ensemble (NVT) simulations to increase temperature up to 2000 K, followed by isothermal-isobaric (NPT) ensemble simulations at high temperature and pressure. After, the systems were slowly quenched to 294 K.

d) The individual units were polymerized, using a nearest-neighbor algorithm (described in previous work),[44] followed by additional relaxation with MD.

e) The NMP was then removed from the system, and the i-PI + IL samples were generated by inserting the IL molecules (anion and cation) in the cavities left by the NMP molecules, again using PACKMOL.

f) A neat i-PI and a composite with the [Tf_2N^-] anion from the previous step were used to produce [BF_4^-] and [PF_6^-] anion based i-PI and i-PI + IL composites. In this

step, all [Tf_2N^-] anions were replaced with the desired anions, while keeping the polymer structure intact. This approach ensures that the i-PI backbone is consistent (same number of polymers and chain lengths), and only the anion composition is changed.

g) Both neat i-PI and i-PI + IL systems were further equilibrated and relaxed via NVT and NPT cycles as mentioned in step (c), until a final temperature of 294 K and a pressure of 1 bar were reached.

All of the MD simulations were performed with the GROMACS 5.0 simulation package.[60] The Lennard-Jones potential and electrostatic interactions were calculated with a cut-off distance of 14.0 Å, and the smooth particle mesh Ewald sum (SPME)[61] method was implemented to calculate long-range electrostatic interactions, with a Fourier spacing of 1.6 Å. The Nose-Hoover thermostat[62] was used to maintain the temperature and the Parrinello-Rahman[63] barostat was used to maintain the pressure, and the time step was 1 fs. In the MD simulations, periodic boundary conditions were implemented in all three dimensions.

In order to estimate the reproducibility of our results, three different independent replicates were separately simulated and evaluated in our structural and adsorption property analysis. A summary of the different i-PI systems is described in Table 1.

Table 1. Summary of different i-PI systems (a → h) simulated.

description (including approximate box length)	# monomers	# NMP	polymer chain lengths*	Average M_w (g/mol)
(a) neat, 6 nm (sample 1)	200	0	17, 8(2), 5(2), 4(6), 3(11), 2(18), 1(64)	5484.3
(b) neat, 6 nm (sample 2)	200	0	76, 56, 29, 20,15, 2(2)	31338.9
(c) neat, 6 nm (sample 4)	200	0	131, 32, 19, 18	54843.1

(d) neat, 6 nm (sample 5)	200	0	94, 30, 28, 16, 15, 8, 5, 4	27421.6
(e) neat, 6 nm (sample 3)	200	800	80, 41, 40, 20, 13, 6	36562.1
(f) composite, 6.8 nm (sample 1)	200 (+ 200 IL)	800	80, 41, 40, 20, 13, 6	36562.1
(g) composite, 6.8 nm (sample 2)	200 (+ 200 IL)	1200	81, 58, 57, 2(2)	43747.5
(h) composite, 6.8 nm (sample 3)	200 (+ 200 IL)	1600	178, 14, 8	73124.1

**Numbers inside the parentheses represent the number of different chains with the same polymer chain length.*

The density of each sample (designated as (a) through (h) from Table 1) is reported in Table 2. For instance, the (a) sample of the [Tf_2N^-]-based neat polymer has the same polymer chain length as the (a) sample in both the [BF_4^-]-based and the [PF_6^-]-based neat polymer as well. The only difference is the type of the anion used to create the neutral monomer (Figure 1).

Table 2. Density (g/cm^3) of neat i-PI and composite of i-PI + IL samples at 1 bar and 294 K. The columns #1 to #5 indicate different independent replicates.

	Mol% IL	#1	#2	#3	#4	#5	Average density
[Tf_2N^-]-based	neat i-PI	1.643 (a)*	1.605 (b)	1.603(e)	1.602 (c)	1.604 (d)	1.612 ± 0.018
	i-PI + 50% IL	1.584 (f)	1.583 (g)	1.585 (h)	-	-	1.584 ± 0.001
	i-PI + 30% IL	1.594 (f)	1.593 (g)	1.595 (h)	-	-	1.594 ± 0.001
	i-PI + 10% IL	1.600 (f)	1.599 (g)	1.599 (h)	-	-	1.600 ± 0.001
[BF_4^-]-based	neat i-PI	1.386 (a)	1.369 (b)	1.372 (e)	1.369 (c)	1.368 (d)	1.373 ± 0.008
	i-PI + 50% IL	1.325 (f)	1.322 (g)	1.326 (h)	-	-	1.324 ± 0.002
	i-PI + 30% IL	1.347 (f)	1.347 (g)	1.346 (h)	-	-	1.347 ± 0.001
	i-PI + 10% IL	1.363 (f)	1.361 (g)	1.362 (h)	-	-	1.362 ± 0.001
[PF_6^-]-based	neat i-PI	1.489 (a)	1.474 (b)	1.474 (e)	-	-	1.479 ± 0.009
	i-PI + 50% IL	1.446 (f)	1.444 (g)	1.447 (h)	-	-	1.446 ± 0.001
	i-PI + 30% IL	1.458 (f)	1.465 (g)	1.460 (h)	-	-	1.461 ± 0.003
	i-PI + 10% IL	1.466 (f)	1.470 (g)	1.478 (h)	-	-	1.471 ± 0.006

**the letter in the parentheses corresponds to the polymer system in Table 1.*

Once the neat i-PI and i-PI + IL samples were prepared, we used the Cassandra simulation package to run GCMC simulations of gas adsorption.[64,65] Each single sample

after preparation was followed by 15 MD/GCMC simulation cycles at 1 bar and 294 K. These relaxation cycles are important, since the adsorbed gas leads to changes in the polymer structure that shift (increase) the predicted equilibrium adsorption. There is negligible swelling of the i-PI system in experiment (due to the low CO_2 loading), so NVT simulations are used during the MD relaxation. During the GCMC simulations, the polymer and IL molecules were held rigid, while the adsorbate molecules were subject to at least 3×10^6 MC steps (33% insertion, 33% deletion, 17% translation, and 17% rotation). In order to improve sampling, these GCMC simulations were iteratively combined with MD simulations to further relax the system configuration. For instance, after finishing one stage of GCMC simulations, the resulting structure (including the gas molecules) was subjected to a short NVT MD relaxation process of 1 ns at the same temperature (294 K). The final structure after these 15 MD/GCMC cycles of equilibration was used for calculating gas selectivity with production runs of 20×10^6 GCMC steps used to calculate averages and error bars. Additional tests were performed with increased MD/GCMC cycles to ensure adequate equilibration and structural relaxation (see Figure S-1 to S-3), and 15 cycles were generally found to be sufficient.

Gas selectivity was calculated for two binary gas mixtures (CO_2/CH_4 and CO_2/N_2), each corresponding to four different gas-phase concentrations (0.5/0.5, 0.2/0.8, 0.1/0.9, 0.05/0.95) and a total pressure of 1 bar and 294 K. The adsorption selectivity is defined as $S = (x_A/y_A)/(x_B/y_B)$, where x_i is the mole fraction of component *i* in the adsorbed phase and y_i is the mole fraction in the gas phase. Two extra samples (#4 and #5) were generated and tested only for [Tf_2N^-] and [BF_4^-] anions, since the [Tf_2N^-]-based structure showed very

high variability for the CO_2/N_2 mixture selectivity, and the [BF_4^-]-based structure showed very high selectivity for CO_2/CH_4, so these extra samples were used to improve confidence.

In order to connect the i-PI and i-PI + IL composite adsorption properties to the underlying molecular configurations, several different structural analyses were performed, which were originally applied to characterize solid adsorbents. Using the approaches of Gelb and Gubbins,[66] we calculated the theoretical FFV, PSD,[67] and exposed surface area for our i-PI and i-PI + IL composite models. Similar information could be generated from publicly available analysis tools like Poreblazer from the Sarkisov group.[68] The structural analyses was performed by including all atomic sites during the analyses, with the Lennard-Jones diameters used to define the molecular surfaces, and in the case of the surface area, the default probe diameter is 4.0 Å. This probe diameter is similar to the kinetic diameters of the gas molecules, but the sensitivity of our results to this particular value is tested. Also, the radial distribution function (RDF) of key interaction sites in the system are analyzed.

3. Results and Discussion

3.1. Gas Solubility

Gas solubility results for different i-PI + IL combinations are reported in Figure S-1 to S-3, corresponding to different stages along the MD/GCMC relxation steps. As mentioned previously, selected systems were run for 15 additional MD/GCMC cycles (also included in Figures S-1 to S-3) to confirm equilibrium saturation values. As Figure 2 shows, the composite structures of the i-PI + ILs show lower gas solubility, regardless of the anion, as compared to the neat polymer (and this is similar to the experimental systems). In the experimental [Tf_2N^-]-based i-PI + IL tests, the CO_2 solubility decreases by 7% and N_2 solubility decreases by 24%, while the CH_4 solubility to relatively constant, as compared

to the neat i-PI.[42] Although not experimentally tested, the simulated CO_2 solubility for the different anion derivatives show the following order: $[PF_6^-] > [BF_4^-] > [Tf_2N^-]$. This trend is also observed for the other gases (N_2 and CH_4) studied in this work. However, the bulk ILs (no i-PI present) show a different trend for CO_2 solubility, as shown in Tables S-1 and S-2 (which compares the solubility and selectivity of several different types of porous adsorbents and ILs from the literature). There are several fundamental differences between our systems and bulk ILs, so it is not surprising that the trends can differ. For instance, with our systems, the bulk ionic liquid structure is completely disrupted, due to the presence of the i-PI (major constituent). Thus, different atomic sites are more or less exposed to the gases, and different geometric cavities can be formed.

The CO_2 solubility of the bulk $[Tf_2N^-]$-based ILs is highest among our selected group of three anions. To explore the origin of the IL effect on solubility in the i-PI + IL composite, several different structural analyses were implemented and discussed in the following.

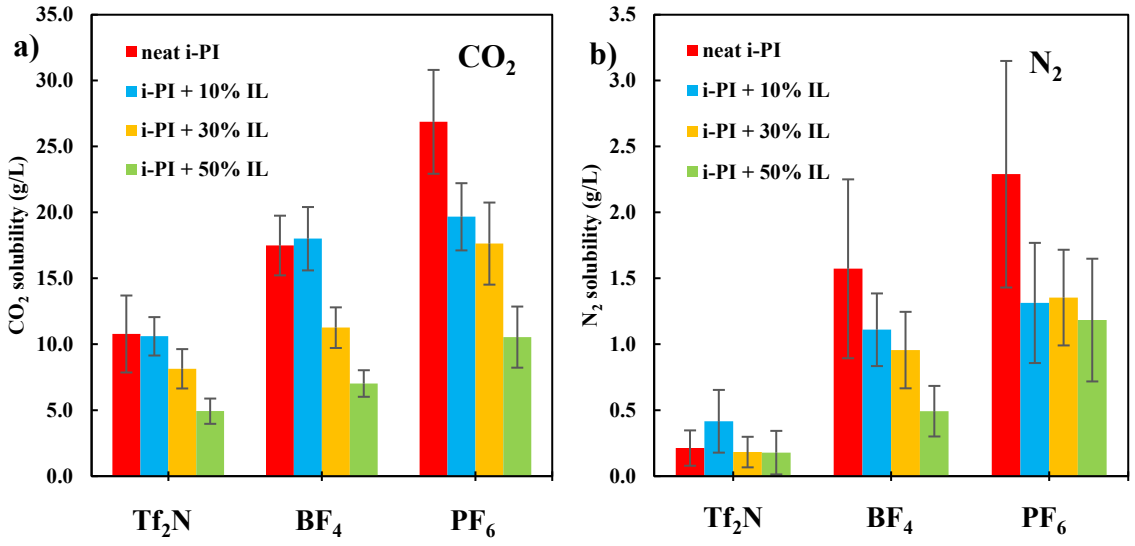

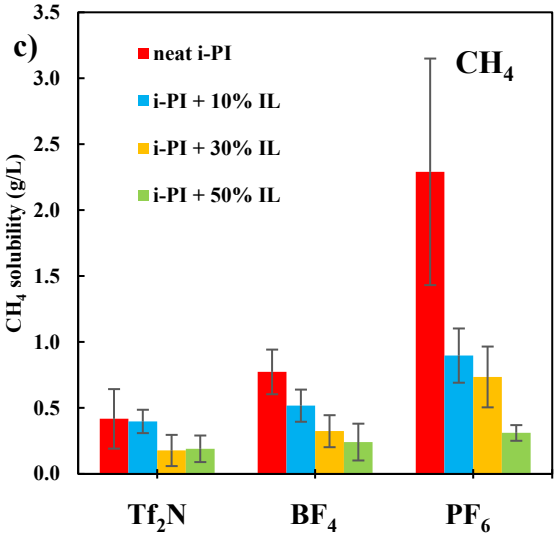

Figure 2. Calculated pure gas solubility at 294 K and 1 bar within neat i-PI and i-PI + IL composites. a) CO_2, b) N_2, and c) CH_4. It should be noted that the scale for CO_2 solubility is ten times higher than that of the other gases.

3.2. Gas Selectivity

The results of gas selectivity for CO_2/CH_4 and CO_2/N_2 mixtures are reported in Figures 3 and 4. While [PF_6^-]-based structures showed higher gas solubility for both neat i-PI and i-PI + IL systems, the [BF_4^-]-based structures show the highest CO_2/CH_4 gas selectivity, which is most relevant to natural gas sweetening applications. To further evaluate [BF_4^-]-based structures and check the reproducibility of the extracted results, two extra samples were prepared. The [PF_6^-]-based structures showed the second best results for CO_2/CH_4 gas selectivity (adding IL in the i-PI enhances the selectivity, while in [Tf_2N^-]-based structures, adding the IL reduces the gas selectivity of CO_2/CH_4. Figure 3 shows a different pattern for gas selectivity in [BF_4^-]-based structures. Neat [BF_4^-]-based i-PI materials show higher selectivity than composite structures with 10% and 30% IL addition. From neat polymer to 10% of IL composite, the selectivity sharply decreases in [BF_4^-]-based

composites. However, upon increasing IL concentration the selectivity will rise back to the neat polymer selectivity value, which occurs at 50 mol% IL concentration.

The gas selectivity calculations of CO_2/N_2 mixtures (Figure 4) show higher uncertainty in comparison to the CO_2/CH_4 results, and this is primarily due to the small number of N_2 species present in the system. The high uncertainty for CO_2/N_2 persists even after doubling the number of GCMC simulation steps. In almost all of the different anion based structures, adding IL does not have a significant positive effect on the gas selectivity for CO_2/N_2 mixtures.

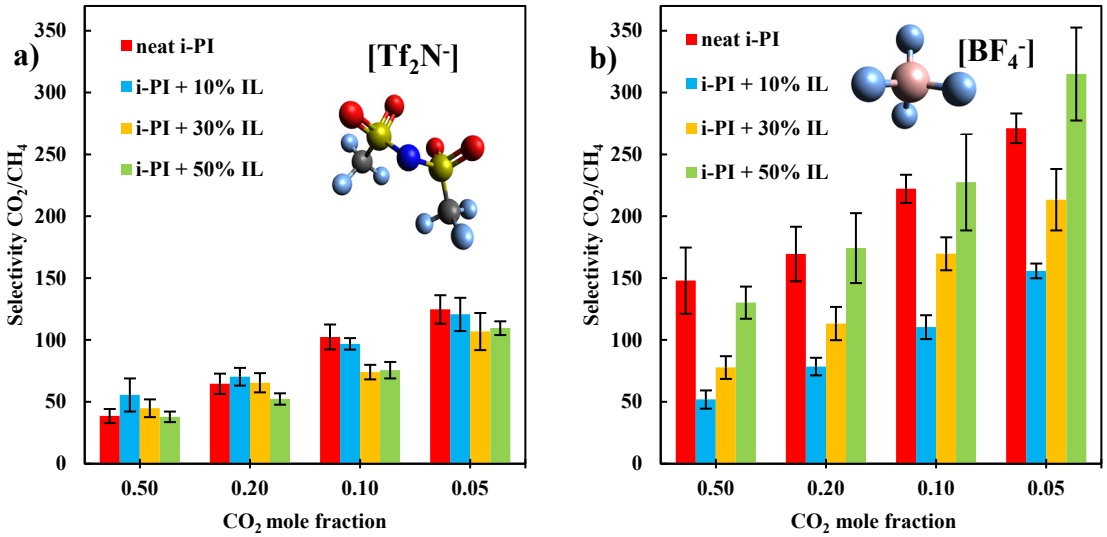

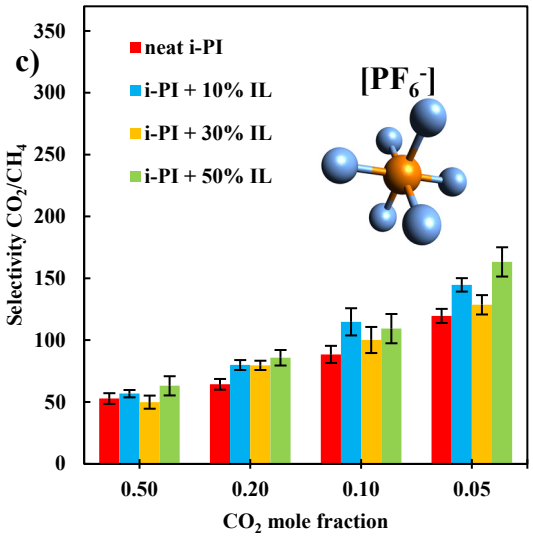

Figure 3. Predicted CO_2/CH_4 selectivity for: a) [Tf_2N^-], b) [BF_4^-], and c) [PF_6^-] at 294 K and 1 bar.

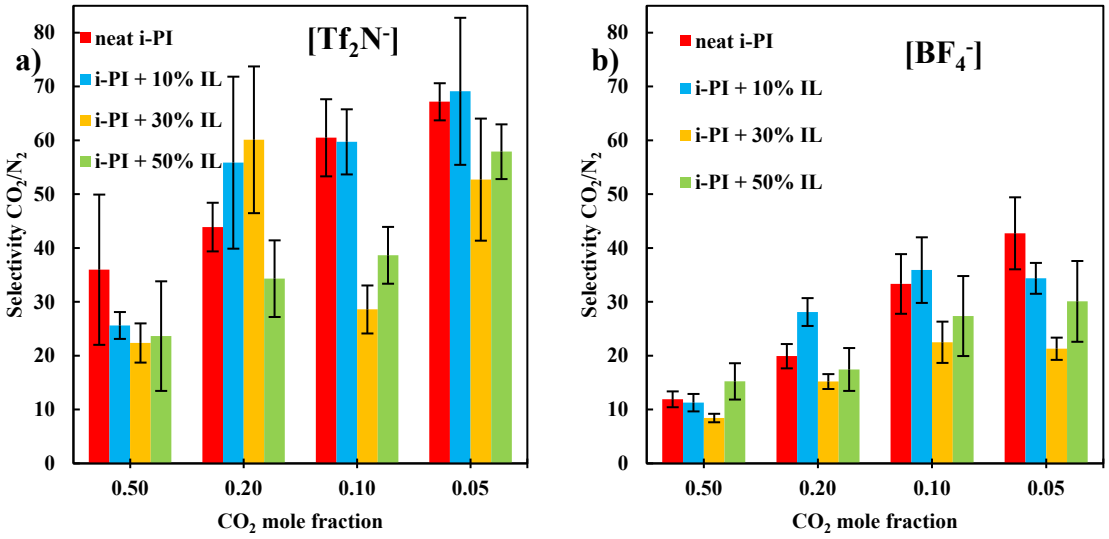

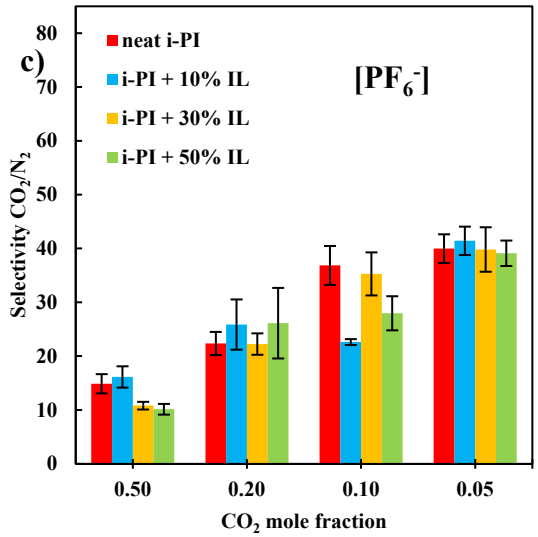

Figure 4. Predicted CO_2/N_2 selectivity for: a) [Tf_2N^-], b) [BF_4^-], and c) [PF_6^-] at 294 K and 1 bar.

3.3. Structural Analysis

A series of structural analyses were used to examine the different i-PI + IL composite compositions and different IL concentrations, in order to establishes clearer correlations with the predicted gas solubility. The resulting structure after CO_2 saturation was printed using a 3D printing tool and presented in Figure S-4. As Figure 5 shows, the pore size distributions demonstrate the high probability of small pores in all systems (radii generally < 1.5 Å). However, the [PF_6^-]-based materials are consistently found to have a slight shift from the smaller pore sizes to the higher end of the size spectrum (> 1.5 Å). In tandem, Figure 6a shows that the [PF_6^-]-based structures also have an elevated surface area, in comparison to other anion-based structures. These structural features (e.g., a higher probability of larger pores and a larger surface area) allow for increased gas adsorption. When comparing all of the different i-PI systems and i-PI + IL composites (Figure 6), we find that gas solubility is strongly correlated with the theoretical surface area of these

materials: [PF_6^-] > [BF_4^-] > [Tf_2N^-]. The surface areas of all composite i-PI + IL structures are less than those of the neat i-PI structures, and this trend mimics the solubility results.

The impact of detailed structural features on the solubility and selectivity of other polymeric materials has been evaluated in some previous computational studies.[69,70] For instance, Wood, et al. previously performed two separate simulation studies on the uptake of both CH_4[71] and H_2[72] in hypercrosslinked organic polymers and compared results with experimental data. The simulated adsorption data, in agreement with experiment, was shown to strongly correlate with the surface area of the material. The two main factors that were determined to govern adsorption in these materials were the micropore volume and surface area. Also, a high coloration between surface area and permeability of PIMs has been previously reported by Madkour and Mark.[69]

The FFV values in our study do not provide a consistent indication of gas solubility for i-PIs, while it has shown to be a sufficient indicator for permeability in previous studies of PIMs.[69,73] As Figure 6b shows, the FFV very slightly increases with respect to the IL addition, but this trend is not mimicked by the solubility. For instance, the [Tf_2N^-]-based structures show the highest FFV, and the [BF_4^-]-based structures show the lowest FFV (similar to the density trend in Table 2). However, the [BF_4^-]-based structures are predicted to have higher gas solubility. In addition, while the [BF_4^-]-based structures have a lower density than the [PF_6^-]-based structures, the gas solubility of [PF_6^-]-based structures is higher. As a result, the density and FFV are not found to correlate well with gas solubility in the present study. While these metrics may be useful for identifying larger differences in other systems, we find that they are not able to adequately capture the subtle structural features in our i-PI and i-PI + IL systems.

Figure 7 shows the structural changes (surface area and FFV) before and after performing the MD/GCMC cycles, in order to map the simultaneous evolution of these system properties. Positive changes in the surface area between the initial and final structures show that adsorbed CO_2 imparts increases in the surface area (while the density is constant throughout all of the MD/GCMC cycles). The small increases in the surface area (~1-4%) correlate with large impacts on the CO_2 solubility (by up to 200%), as shown in Figure 7b. However, FFV does not show significant changes. In fact, FFV decreases in half of the cases, indicating a clear inconsistency with respect to the CO_2 solubility.

The accessible surface area calculation is strongly dependent upon the probe size used, and this can potentially be a major factor in our analysis and comparison. In particular, we are working with three different gases (CO_2, N_2, and CH_4 with kinetic diameters of 3.30, 3.64, 3.80 Å, respectively).[74-76] To explore this issue, a range of different probe sizes were tested in the surface area calculation, with the resulting surface areas shown in Figure 8 (a default value of 4.0 Å was used in Figure 6). Regardless of the probe size used, the [PF_6^-]-based structures show the highest surface area, and the [Tf_2N^-]-based structures show the lowest. Using a probe diameter of 1.0 Å, the calculated surface area of the composite structures is higher than that of the neat polymer. Also when using this small probe size, the surface area is predicted to increase as the concentration of the IL increases (in contrast to the trend predicted with the larger probes). However, a probe diameter of 1.0 Å is able to explore large regions of the material that are likely inaccessible and irrelevant to our adsorbates.

Another interesting result is the surface area of the i-PI + 10% IL in [Tf_2N^-]-based and [BF_4^-]-based systems, as there is a large probe-size dependency. As Figures 8c and 8d

show, with a probe size larger than 3.0 Å, the surface area of the i-PI + 10% IL composite is larger than the neat i-PI. With a probe diameter of 2.0 Å, the surface areas of the neat and composite (10% IL) structures are almost overlapping. However, as the probe size grows from 3.0 to 4.0 Å, the gap between neat and composite (10% IL) increases in favor of the composite structure. This surface area analysis indicates that the composite structures have a higher probability of smaller pore sizes, and this further corroborates the PSD analysis in Figure 5.

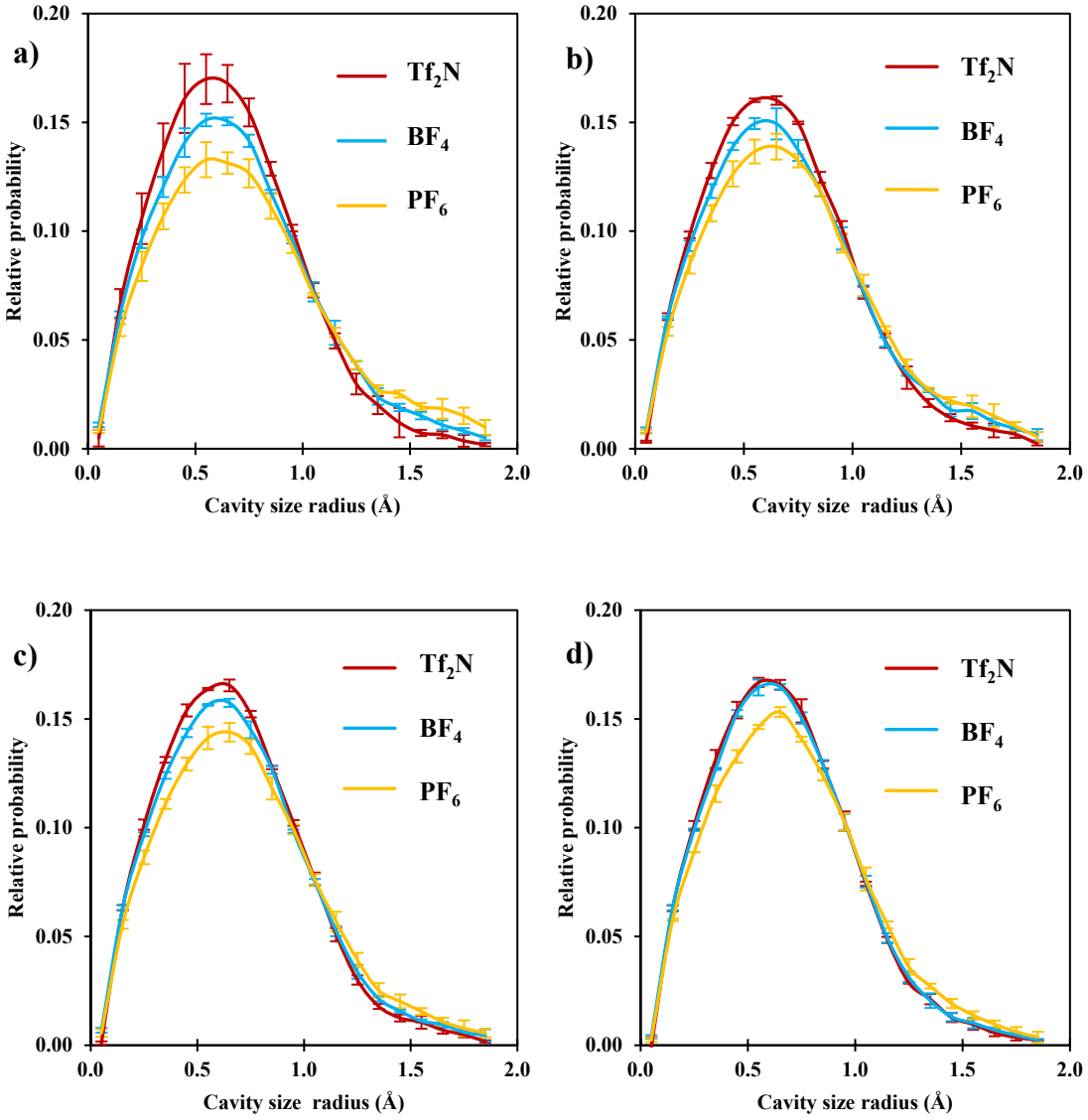

Figure 5. Pore size distribution for: a) neat i-PI, b) composite structure of i-PI + 10% IL, c) i-PI + 30% IL, and d) i-PI + 50% IL at 294 K and 1 bar (specifically, sample #2 of Table 2 after CO_2 saturation).

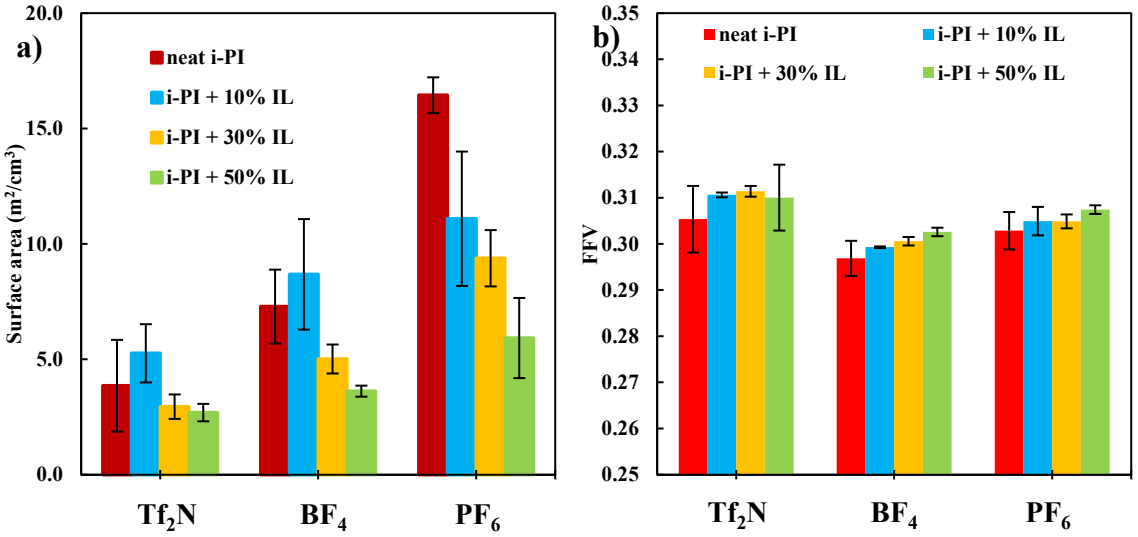

Figure 6. Comparison of: a) the surface area and b) the FFV at 294 K and 1 bar for CO_2 saturated structures.

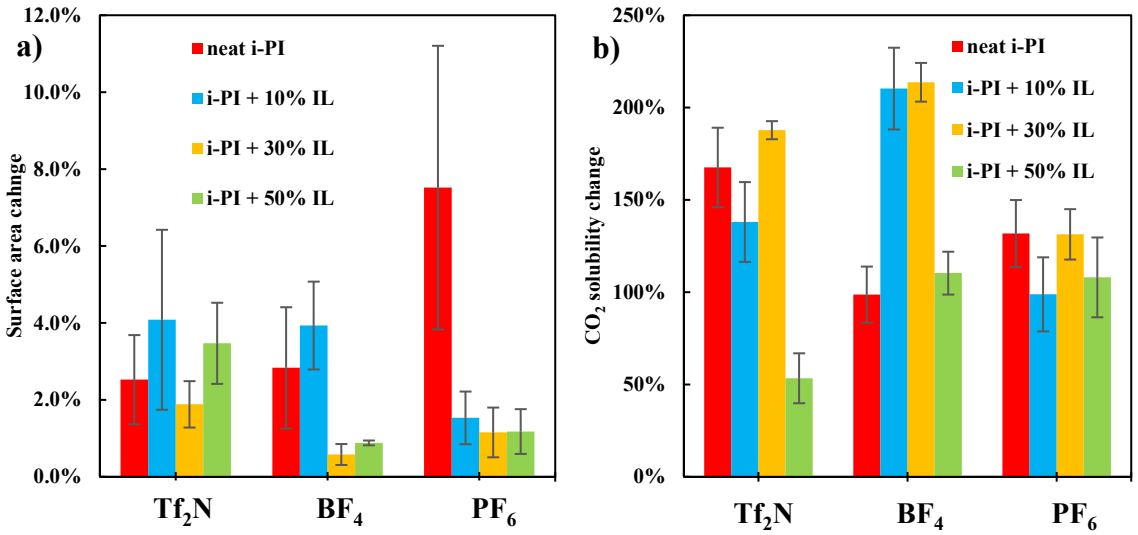

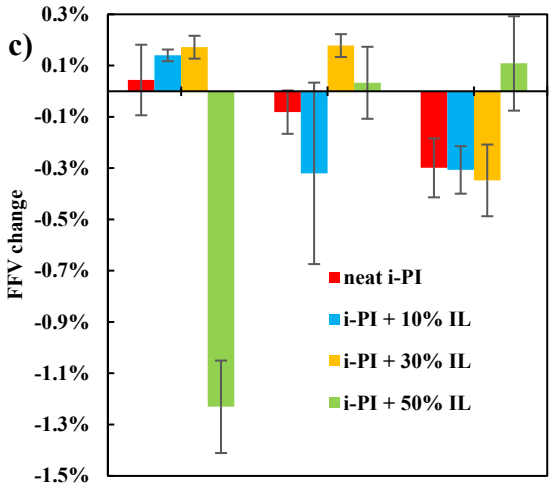

Figure 7. Comparison of the average: a) surface area, b) solubility, and c) FFV change before and after the MD/GCMC cycles involving CO_2 adsorption.

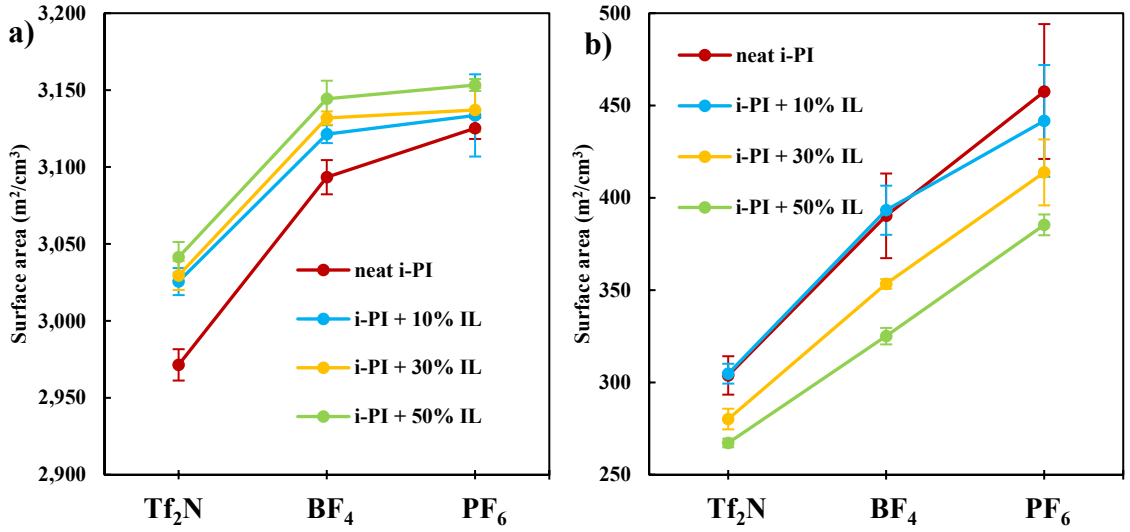

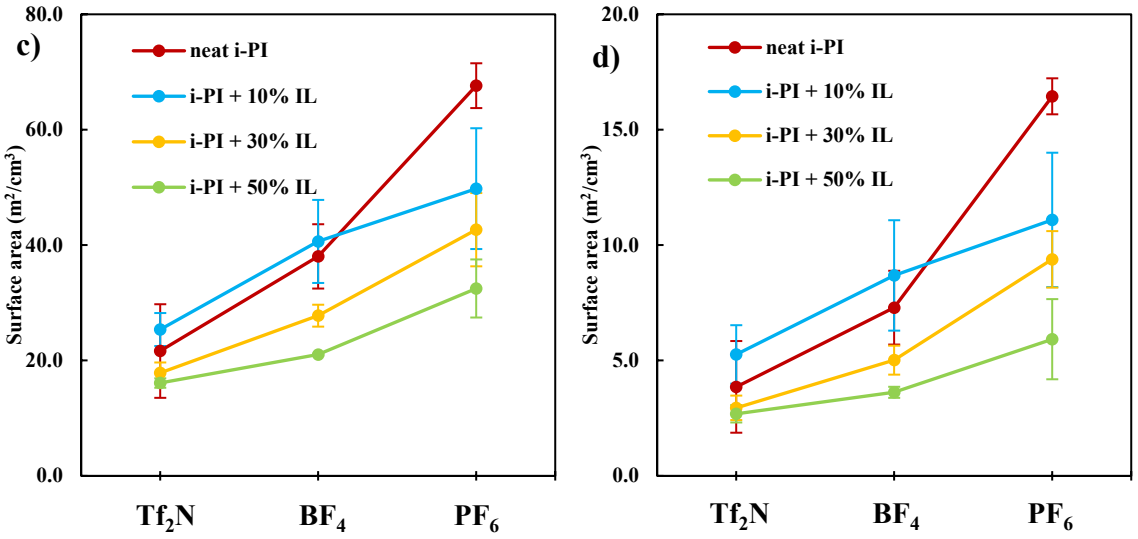

Figure 8. Probe diameter size sensitivity analysis for the CO_2 saturated structures: a) 1.0 Å, b) 2.0 Å, c) 3.0 Å, and d) 4.0 Å.

3.4. Adsorbate/Adsorbent Interaction Analysis

To identify the dominant molecular-level interactions involved with the gas adsorption, radial distribution functions were calculated for key sites in our i-PI and i-PI + IL systems. In general, the RDF represents the average of three samples from 10 ns of NVT MD simulation at 294 K. The carbon atoms of CO_2 and CH_4 molecules and the nitrogen atoms of N_2 gas molecules were chosen to represent the molecular adsorbate interactions with different sites of the adsorbents. With respect to the different anions, the boron (B) atoms in [BF_4^-], the phosphorus (P) atoms in [PF_6^-], and the oxygen (O) atoms in [Tf_2N^-] molecules were selected to represent the anions in the RDF calculation since CO_2 molecules show a strong interaction with the oxygen sites of the [Tf_2N^-]. The different nitrogen sites of the monomer are identified in Figure 1. The N1 and N2 nitrogen on the monomer represent the ligand sites of the polymer and N3 to N6 were identified as imidazolium ring nitrogen atoms in the polymer structure.

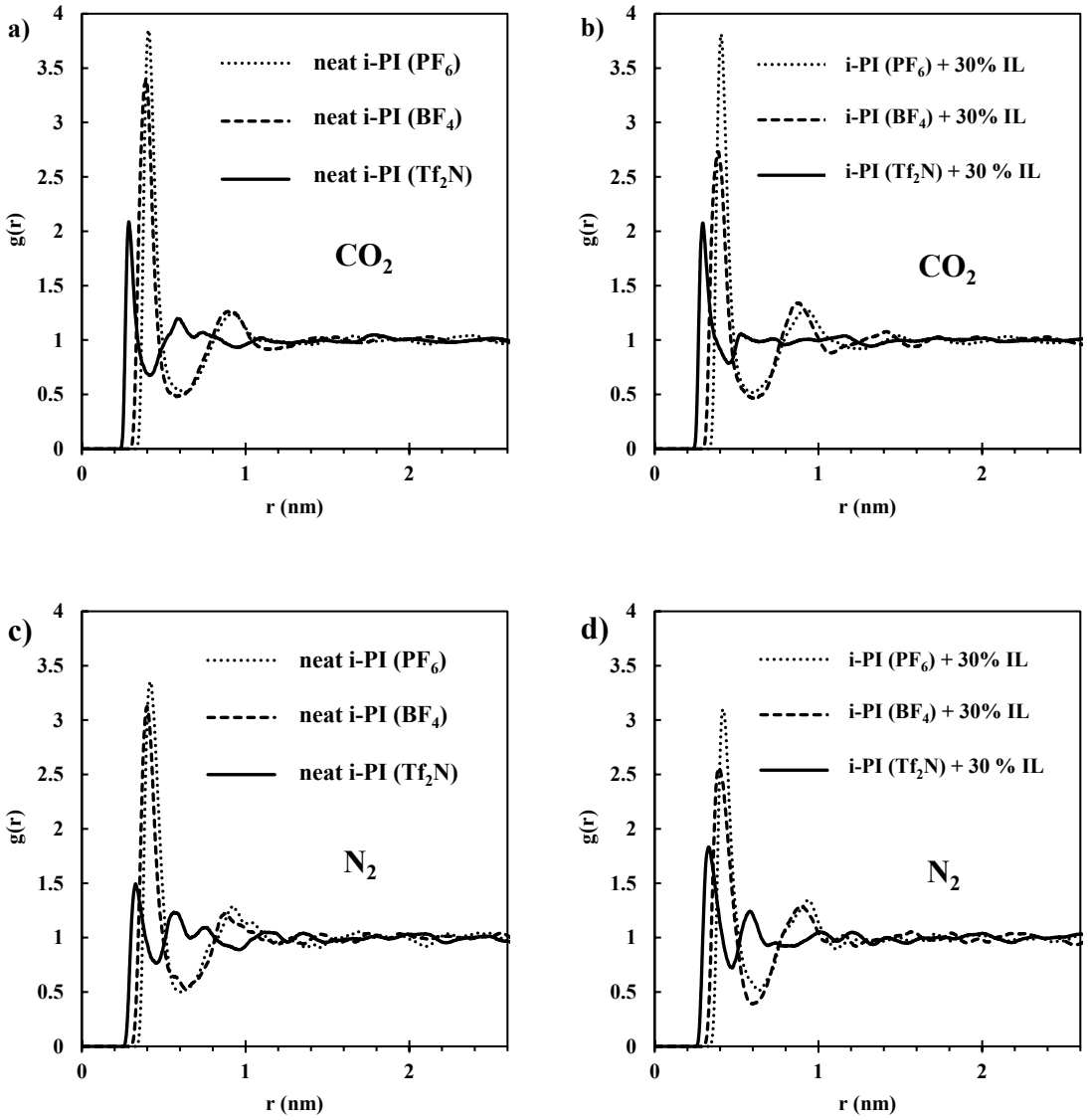
a)
neat i-PI (PF_6)
neat i-PI (BF_4)
neat i-PI (Tf_2N)
CO_2
b)
i-PI (PF_6) + 30% IL
i-PI (BF_4) + 30% IL
i-PI (Tf_2N) + 30 % IL
CO_2
c)
neat i-PI (PF_6)
neat i-PI (BF_4)
neat i-PI (Tf_2N)
N_2
d)
i-PI (PF_6) + 30% IL
i-PI (BF_4) + 30% IL
i-PI (Tf_2N) + 30 % IL
N_2
g(r)
r (nm)

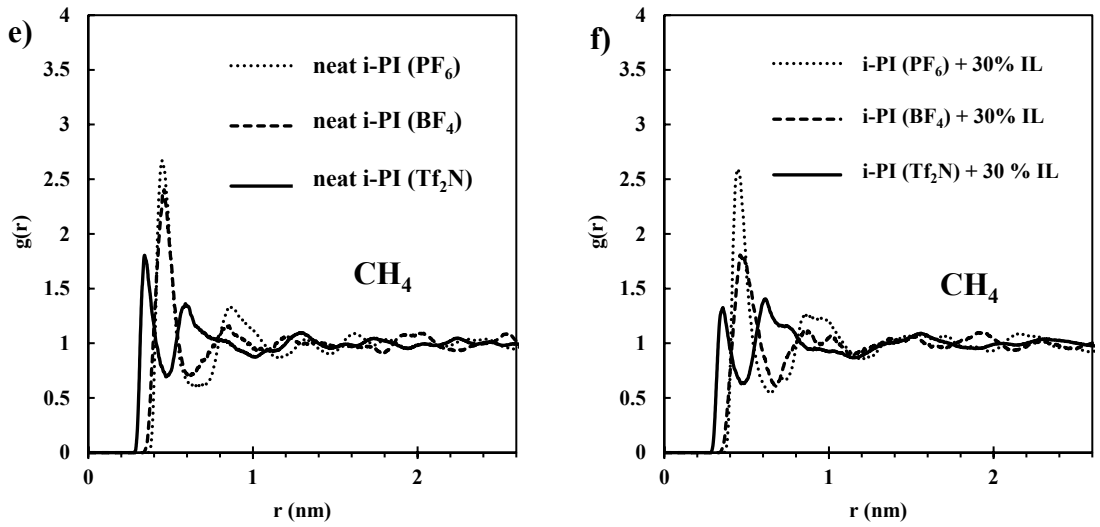

Figure 9. Radial distribution functions of gas interactions with different anion species: a and b) carbon site of CO_2; c and d) nitrogen sites of N_2 ; e and f) carbon site of CH_4.

Figure 9 represents the adsorbed gas interactions with different anions. In general, the interaction intensity (height of the first peak in the RDF) of different anions with the adsorbed gases shows the following trend: $[PF_6^-] > [BF_4^-] > [Tf_2N^-]$. The strongest gas interaction was observed with the $[PF_6^-]$ anions, and this is consistent, regardless of the different gas types and different IL concentrations within the polymer + IL composites. With respect to the different gas species, the height of the first RDF peak follows the trend: $CO_2 > N_2 > CH_4$ in almost all concentrations of polymer + IL.

The interaction of the adsorbed CO_2 with $[Tf_2N^-]$ and $[PF_6^-]$ remains constant in the neat i-PI structure and in the i-PI + IL composites (Figures S-5 to S-7). The interaction of CO_2 with $[BF_4^-]$ is reduced in the i-PI + 10% and i-PI + 30% IL, while the interactions increases back to the original value in the i-PI + 50% IL.

The N_2 molecules show very similar behavior to the CO_2 molecules, with respect to their interaction with the anions. Adding IL to the i-PI does not significantly change the N_2 gas molecule interactions within the [Tf_2N^-] and [PF_6^-]-based structures. However, the N_2 gas molecules within the [BF_4^-]-based structures show a weakened interaction with the [BF_4^-] anions from the addition of 10% and 30 % IL. In the polymer + 50% IL samples, the interaction rises back to the value observed in the neat i-PI.

The interactions of CH_4 with the anions are characteristically different from those of the CO_2 and N_2 gas molecules. In the [Tf_2N^-] and [BF_4^-]-based structures, the CH_4 interaction with the anions decreases with the addition of the IL. In the i-PI + 50% IL in [BF_4^-]-based structures, the CH_4 and anion interaction returns to the value found within the neat polymer. In the [PF_6^-]-based structures, the CH_4 interaction with the anions remains constant, despite IL addition to the polymer.

While the changes in adsorption and site-site specificity are moderate, these details provide fundamental insight into further tuning the gas selectivity of mixed i-PI + IL composite systems. While other site-site interactions were investigated (such as different sites of i-PI backbone and [C_4mim^+] species), our primary focus of this investigation and the largest changes are found to be associated with the anions.

4. Conclusion

In this study, the gas selectivity of different combinations of anions in a composite (i-PI + IL) material are evaluated, and the performance is analyzed with respect to detailed structural changes and specific molecular interactions. The positive charge of the monomer backbone is compensated by paring with different anions ([PF_6^-], [BF_4^-], and [Tf_2N^-]) to

yield a charge neutral i-PI structure. Additionally, different composite structures of the i-PI + IL ([C_4mim^+] with [PF_6^-], [BF_4^-], and [Tf_2N^-]) were investigated to evaluate the effect of the IL on gas solubility and selectivity for each structure.

While [PF_6^-]-based structures (neat i-PI and i-PI + IL composites) showed the highest CO_2 solubility, [BF_4^-]-based structures showed the highest selectivity for CO_2 from the CO_2/CH_4 mixture. Comparing the initial and equilibrated structures of the prepared samples reveals that the CO_2 adsorption leads to notable changes in the structure. A high surface area as well as a high probability of larger pore sizes increases the gas solubility, while adding IL to the neat polymer system reduces the surface area and decreases the gas solubility, and this is consistent with experiments. The surface area follows the same trend for three different anion based structures: [PF_6^-] > [BF_4^-] > [Tf_2N^-]. The composite structure of neat i-PI + IL also switches the adsorption sites in the polymer structure for the CO_2/CH_4 gas mixture from ligand to imidazolium sites.

In our previous work,[44] pure CH_4 displays a stronger interaction with the neat [Tf_2N^-]-based i-PI in comparison to the CO_2 gas. However, upon adding IL, the CH_4:anion interaction showed a sharp decrease in the i-PI + IL composite structure. This current study supports the previous work and explains the competitive occupation and interaction between mixed gas adsorption. The CO_2 has a stronger interaction with the anion in all of the neat i-PI and i-PI + IL composites. Although the [PF_6^-]-based structure has higher gas solubility (due to larger pores and surface area), the selectivity remains a challenging issue. Experimental investigations are currently underway to corroborate the trends found in the current study and it has been verified that i-PIs with each anion can be readily synthesized from the corresponding Cl- salt, although i-PIs with BF_4^- and PF_6^- anions form much more

brittle films than those with Tf_2N^- anions. We are also exploring how the nature of the IL additive influences gas permeability and separation by utilizing the different cations such as 1-ethyl-3-methylimidazolium ([C_2mim^+]) or 1-benzyl-3-methylimidazolium ([$Bnmim^+$]).

Acknowledgements

Support for this work was provided by: National Science Foundation (CBET-1605411); Department of Energy Basic Energy Sciences (DE-SC0018181); Computer resources were provided by the Alabama Supercomputer Center.

Supplementary Data

MD/GCMC cycles of the CO_2 solubility, 3D printed structure, CO_2 solubility capacity comparison with other polymers and porous materials, RDF calculation of anion and adsorbed gas (CO_2, CH_4, and N_2) interactions for all concentrations of i-PI + IL composite structures.

References

(1) Martín, C. F.; Stöckel, E.; Clowes, R.; Adams, D. J.; Cooper, A. I.; Pis, J. J.; Rubiera, F.; Pevida, C. Hypercrosslinked organic polymer networks as potential adsorbents for pre-combustion CO_2 capture. *J. Mater. Chem.* **2011**, *21*, 5475-5483.

(2) Abdul Halim, H. N.; M. Shariff, A.; Tan, L. S.; Bustam, M. A. Mass Transfer Performance of CO_2 Absorption from Natural Gas using Monoethanolamine (MEA) in High Pressure Operations. *Ind. Eng. Chem. Res.* **2015**, *54*, 1675-1680.

(3) To, J. W.; He, J.; Mei, J.; Haghpanah, R.; Chen, Z.; Kurosawa, T.; Chen, S.; Bae, W. G.; Pan, L.; Tok, J. B.; Wilcox, J.; Bao, Z. Hierarchical N-Doped Carbon as CO_2 Adsorbent with High CO_2 Selectivity from Rationally Designed Polypyrrole Precursor. *J. Am. Chem. Soc.* **2016**, *138*, 1001-1009.

(4) Delgado, J. A.; Águeda, V. I.; Uguina, M. A.; Sotelo, J. L.; Brea, P.; Grande, C. A. Adsorption and Diffusion of H_2, CO, CH_4, and CO_2 in BPL Activated Carbon and 13X Zeolite: Evaluation of Performance in Pressure Swing Adsorption Hydrogen Purification by Simulation. *Ind. Eng. Chem. Res.* **2014**, *53*, 15414-15426.

(5) Vicent-Luna, J. M.; Luna-Triguero, A.; Calero, S. Storage and Separation of Carbon Dioxide and Methane in Hydrated Covalent Organic Frameworks. *J. Phys. Chem. C* **2016**, *120*, 23756-23762.

(6) Xiang, Z.; Mercado, R.; Huck, J. M.; Wang, H.; Guo, Z.; Wang, W.; Cao, D.; Haranczyk, M.; Smit, B. Systematic Tuning and Multifunctionalization of Covalent Organic Polymers for Enhanced Carbon Capture. *J. Am. Chem. Soc.* **2015**, *137*, 13301-13307.

(7) Zeng, S.; Zhang, X.; Bai, L.; Zhang, X.; Wang, H.; Wang, J.; Bao, D.; Li, M.; Liu, X.; Zhang, S. Ionic-Liquid-Based CO_2 Capture Systems: Structure, Interaction and Process. *Chem. Rev.* **2017**, *117*, 9625-9673.

(8) Budhathoki, S.; Shah, J. K.; Maginn, E. J. Molecular Simulation Study of the Performance of Supported Ionic Liquid Phase Materials for the Separation of Carbon Dioxide from Methane and Hydrogen. *Ind. Eng. Chem. Res.* **2017**, *56*, 6775-6784.

(9) Cadena, C.; Anthony, J. L.; Shah, J. K.; Morrow, T. I.; Brennecke, J. F.; Maginn, E. J. Why is CO_2 so soluble in imidazolium-based ionic liquids? *J. Am. Chem. Soc.* **2004**, *126*, 5300-5308.

(10) Sezginel, K. B.; Keskin, S.; Uzun, A. Tuning the Gas Separation Performance of CuBTC by Ionic Liquid Incorporation. *Langmuir* **2016**, *32*, 1139-1147.

(11) Li, Z.; Xiao, Y.; Xue, W.; Yang, Q.; Zhong, C. Ionic Liquid/Metal–Organic Framework Composites for H2S Removal from Natural Gas: A Computational Exploration. *J. Phys. Chem. C* **2015**, *119*, 3674-3683.

(12) Harris, K. R.; Kanakubo, M. Self-diffusion, velocity cross-correlation, distinct diffusion and resistance coefficients of the ionic liquid [BMIM][Tf_2N] at high pressure. *Phys. Chem. Chem. Phys.* **2015**, *17*, 23977-23993.

(13) Kinik, F. P.; Altintas, C.; Balci, V.; Koyuturk, B.; Uzun, A.; Keskin, S. [BMIM][PF_6] Incorporation Doubles CO_2 Selectivity of ZIF-8: Elucidation of Interactions and Their Consequences on Performance. *ACS Appl. Mater. Inter.* **2016**, *8*, 30992-31005.

(14) Wu, N.; Ji, X.; Xie, W.; Liu, C.; Feng, X.; Lu, X. Confinement Phenomenon Effect on the CO_2 Absorption Working Capacity in Ionic Liquids Immobilized into Porous Solid Supports. *Langmuir* **2017**, *33*, 11719-11726.

(15) Xue, W.; Li, Z.; Huang, H.; Yang, Q.; Liu, D.; Xu, Q.; Zhong, C. Effects of ionic liquid dispersion in metal-organic frameworks and covalent organic frameworks on CO_2 capture: A computational study. *Chem. Eng. Sci.* **2016**, *140*, 1-9.

(16) Shi, W.; Luebke, D. R. Enhanced gas absorption in the ionic liquid 1-n-hexyl-3-methylimidazolium bis(trifluoromethylsulfonyl)amide ([hmim][Tf_2N]) confined in silica slit pores: a molecular simulation study. *Langmuir* **2013**, *29*, 5563-5572.

(17) Vicent-Luna, J. M.; Gutiérrez-Sevillano, J. J.; Anta, J. A.; Calero, S. Effect of Room-Temperature Ionic Liquids on CO_2 Separation by a Cu-BTC Metal–Organic Framework. *J. Phys. Chem. C* **2013**, *117*, 20762-20768.

(18) Kohler, F. T. U.; Popp, S.; Klefer, H.; Eckle, I.; Schrage, C.; Böhringer, B.; Roth, D.; Haumann, M.; Wasserscheid, P. Supported ionic liquid phase (SILP) materials for removal of hazardous gas compounds – efficient and irreversible NH_3 adsorption. *Green Chem.* **2014**, *16*, 3560-3568.

(19) Abedini, A.; Ludwig, T.; Zhang, Z.; Turner, C. H. Molecular Dynamics Simulation of Bismuth Telluride Exfoliation Mechanisms in Different Ionic Liquid Solvents. *Langmuir* **2016**, *32*, 9982-9992.

(20) Tang, Z.; Lu, L.; Dai, Z.; Xie, W.; Shi, L.; Lu, X. CO_2 Absorption in the Ionic Liquids Immobilized on Solid Surface by Molecular Dynamics Simulation. *Langmuir* **2017**, *33*, 11658-11669.

(21) Shen, Y.; Hung, F. R. A Molecular Simulation Study of Carbon Dioxide Uptake by a Deep Eutectic Solvent Confined in Slit Nanopores. *J. Phys. Chem. C* **2017**, *121*, 24562-24575.

(22) Zhang, K.; Kumar, S. K. Molecular Simulations of Solute Transport in Polymer Melts. *ACS Macro Lett.* **2017**, *6*, 864-868.

(23) Wang, M.; Zhao, J.; Wang, X.; Liu, A.; Gleason, K. K. Recent progress on submicron gas-selective polymeric membranes. *J. Mater. Chem. A* **2017**, *5*, 8860-8886.

(24) Tome, L. C.; Marrucho, I. M. Ionic liquid-based materials: a platform to design engineered CO_2 separation membranes. *Chem. Soc. Rev.* **2016**, *45*, 2785-2824.

(25) Rukmani, S. J.; Liyana-Arachchi, T. P.; Hart, K. E.; Colina, C. M. Ionic-Functionalized Polymers of Intrinsic Microporosity for Gas Separation Applications. *Langmuir* **2018**, *34*, 3949-3960.

(26) Sharma, P.; Chakrabarty, S.; Roy, S.; Kumar, R. Molecular View of CO_2 Capture by Polyethylenimine: Role of Structural and Dynamical Heterogeneity. *Langmuir* **2018**, *34(17)*, 5138-5148.

(27) Ma, C.; Urban, J. J. Polymers of Intrinsic Microporosity (PIMs) Gas Separation Membranes: A mini Review. *P. Nat. Res. Soc.* **2018**, *2*, 02002.

(28) Saleh, M.; Lee, H. M.; Kemp, K. C.; Kim, K. S. Highly stable CO_2/N_2 and CO_2/CH_4 selectivity in hyper-cross-linked heterocyclic porous polymers. *ACS Appl. Mater. Inter.* **2014**, *6*, 7325-7333.

(29) Wu, D.; Xu, F.; Sun, B.; Fu, R.; He, H.; Matyjaszewski, K. Design and preparation of porous polymers. *Chem. Rev.* **2012**, *112*, 3959-4015.

(30) Meng, B.; Li, H.; Mahurin, Shannon M.; Liu, H.; Dai, S. Hyper-crosslinked cyclodextrin porous polymer: an efficient CO_2 capturing material with tunable porosity. *RSC Adv.* **2016**, *6*, 110307-110311.

(31) Zhang, B.; Li, G.; Yan, J.; Wang, Z. Tetraphenyladamantane-Based Microporous Polybenzimidazoles for Adsorption of Carbon Dioxide, Hydrogen, and Organic Vapors. *J. Phys. Chem. C* **2015**, *119*, 13080-13087.

(32) Fujii, K.; Ueki, T.; Hashimoto, K.; Kobayashi, Y.; Kitazawa, Y.; Hirosawa, K.; Matsugami, M.; Ohara, K.; Watanabe, M.; Shibayama, M. Microscopic Structure of Solvated Poly(benzyl methacrylate) in an Imidazolium-Based Ionic Liquid: High-Energy X-ray Total Scattering and All-Atom MD Simulation Study. *Macromolecules* **2017**, *50*, 4780-4786.

(33) Ashourirad, B.; Sekizkardes, A. K.; Altarawneh, S.; El-Kaderi, H. M. Exceptional Gas Adsorption Properties by Nitrogen-Doped Porous Carbons Derived from Benzimidazole-Linked Polymers. *Chem. Mater.* **2015**, *27*, 1349-1358.

(34) Errahali, M.; Gatti, G.; Tei, L.; Paul, G.; Rolla, G. A.; Canti, L.; Fraccarollo, A.; Cossi, M.; Comotti, A.; Sozzani, P.; Marchese, L. Microporous Hyper-Cross-Linked Aromatic Polymers Designed for Methane and Carbon Dioxide Adsorption. *J. Phys. Chem. C* **2014**, *118*, 28699-28710.

(35) Ishiwari, F.; Takeuchi, N.; Sato, T.; Yamazaki, H.; Osuga, R.; Kondo, J. N.; Fukushima, T. Rigid-to-Flexible Conformational Transformation: An Efficient Route to Ring-Opening of a Tröger's Base-Containing Ladder Polymer. *ACS Macro Lett.* **2017**, *6*, 775-780.

(36) Gouveia, A. S. L.; Tome, L. C.; Lozinskaya, E. I.; Shaplov, A. S.; Vygodskii, Y. S.; Marrucho, I. M. Exploring the effect of fluorinated anions on the CO_2/N_2 separation of supported ionic liquid membranes. *Phys. Chem. Chem. Phys.* **2017**, *19*, 28876-28884.

(37) Tiwari, R. R.; Jin, J.; Freeman, B. D.; Paul, D. R. Physical aging, CO_2 sorption and plasticization in thin films of polymer with intrinsic microporosity (PIM-1). *J. Membrane Sci.* **2017**, *537*, 362-371.

(38) Shin, J. Y.; Yamada, S. A.; Fayer, M. D. Carbon Dioxide in a Supported Ionic Liquid Membrane: Structural and Rotational Dynamics Measured with 2D IR and Pump-Probe Experiments. *J. Am. Chem. Soc.* **2017**, *139*, 11222-11232.

(39) Cao, B.; Yan, W.; Wang, J.; Ding, H.; Yu, Y. Absorption of CO_2 with supported imidazolium-based ionic liquid membranes. *J. Chem. Technol. Biot.* **2015**, *90*, 1537-1544.

(40) Noble, R. D.; Gin, D. L. Perspective on ionic liquids and ionic liquid membranes. *J. Membrane Sci.* **2011**, *369*, 1-4.

(41) Wang, X.; Akhmedov, N. G.; Duan, Y.; Luebke, D.; Hopkinson, D.; Li, B. Amino acid-functionalized ionic liquid solid sorbents for post-combustion carbon capture. *ACS Appl. Mater. Inter.* **2013**, *5*, 8670-8677.

(42) Mittenthal, M. S.; Flowers, B. S.; Bara, J. E.; Whitley, J. W.; Spear, S. K.; Roveda, J. D.; Wallace, D. A.; Shannon, M. S.; Holler, R.; Martens, R.; Daly, D. T. Ionic Polyimides: Hybrid Polymer Architectures and Composites with Ionic Liquids for Advanced Gas Separation Membranes. *Ind. Eng. Chem. Res.* **2017**, *56*, 5055-5069.

(43) Bonakala, S.; Balasubramanian, S. Structure-Property Relationships in Amorphous Microporous Polymers. *J. Phys. Chem. B* **2016**, *120*, 557-565.

(44) Abedini, A.; Crabtree, E.; Bara, J. E.; Turner, C. H. Molecular Simulation of Ionic Polyimides and Composites with Ionic Liquids as Gas-Separation Membranes. *Langmuir* **2017**, *33*, 11377-11389.

(45) Morozova, S. M.; Shaplov, A. S.; Lozinskaya, E. I.; Mecerreyes, D.; Sardon, H.; Zulfiqar, S.; Suárez-García, F.; Vygodskii, Y. S. Ionic Polyurethanes as a New Family of Poly(ionic liquid)s for Efficient CO_2 Capture. *Macromolecules* **2017**, *50*, 2814-2824.

(46) Qian, W.; Texter, J.; Yan, F. Frontiers in poly(ionic liquid)s: syntheses and applications. *Chem. Soc. Rev.* **2017**, *46*, 1124-1159.

(47) Lu, X. Q.; Qiao, Y. Q.; He, J. R.; Pan, M.; Kang, B. S.; Su, C. Y. Triple-stranded helical and plywood-like arrays: Two uncommon framework isomers based on the common one-dimensional chain structures. *Cryst. Growth Des.* **2006**, *6*, 1910-1914.

(48) Becke, A. D. Density-functional thermochemistry. III. The role of exact exchange. *J. Chem. Phys.* **1993**, *98*, 5648-5652.

(49) Frisch, M. J.; Trucks, G. W.; Schlegel, H. B.; Scuseria, G. E.; Robb, M. A.; Cheeseman, J. R.; Scalmani, G.; Barone, V.; Mennucci, B.; Petersson, G. A.; Nakatsuji, H.; Caricato, M.; Li, X.; Hratchian, H. P.; Izmaylov, A. F.; Bloino, J.; Zheng, G.; Sonnenberg, J. L.; Hada, M.; Ehara, M.; Toyota, K.; Fukuda, R.; Hasegawa, J.; Ishida, M.; Nakajima, T.; Honda, Y.; Kitao, O.; Nakai, H.; Vreven, T.; Montgomery Jr., J. A.; Peralta, J. E.; Ogliaro, F.; Bearpark, M. J.; Heyd, J.; Brothers, E. N.; Kudin, K. N.; Staroverov, V. N.; Kobayashi, R.; Normand, J.; Raghavachari, K.; Rendell, A. P.; Burant, J. C.; Iyengar, S. S.; Tomasi, J.; Cossi, M.; Rega, N.; Millam, N. J.; Klene, M.; Knox, J. E.; Cross, J. B.; Bakken, V.; Adamo, C.; Jaramillo, J.; Gomperts, R.; Stratmann, R. E.; Yazyev, O.; Austin, A. J.; Cammi, R.; Pomelli, C.; Ochterski, J. W.; Martin, R. L.; Morokuma, K.; Zakrzewski, V. G.; Voth, G. A.; Salvador, P.; Dannenberg, J. J.; Dapprich, S.; Daniels, A. D.; Farkas, Ö.; Foresman, J. B.; Ortiz, J. V.; Cioslowski, J.; Fox, D. J.: Gaussian 09. Gaussian, Inc.: Wallingford, CT, USA, 2009.

(50) Lopes, J. N. C.; Padua, A. A. H. Molecular force field for ionic liquids composed of triflate or bistriflylimide anions. *J. Phys. Chem. B* **2004**, *108*, 16893-16898.

(51) Lopes, J. N. C.; Deschamps, J.; Padua, A. A. H. Modeling ionic liquids using a systematic all-atom force field. *J. Phys. Chem. B* **2004**, *108*, 2038-2047.

(52) Resende Prado, C. E.; Gomide Freitas, L. C. Molecular dynamics simulation of the room-temperature ionic liquid 1-butyl-3-methylimidazolium tetrafluoroborate. *J. Mol. Struct.: THEOCHEM* **2007**, *847*, 93-100.

(53) Aparicio, S.; Alcalde, R.; Davila, M. J.; Garcia, B.; Leal, J. M. Measurements and predictive models for the N-methyl-2-pyrrolidone/water/methanol system. *J. Phys. Chem. B* **2008**, *112*, 11361-11373.

(54) Potoff, J. J.; Siepmann, J. I. Vapor-liquid equilibria of mixtures containing alkanes, carbon dioxide, and nitrogen. *AIChE J.* **2001**, *47*, 1676-1682.

(55) Trinh, T. T.; Vlugt, T. J.; Kjelstrup, S. Thermal conductivity of carbon dioxide from non-equilibrium molecular dynamics: a systematic study of several common force fields. *J. Chem. Phys.* **2014**, *141*, 134504-134507.

(56) Budhathoki, S.; Shah, J. K.; Maginn, E. J. Molecular Simulation Study of the Solubility, Diffusivity and Permselectivity of Pure and Binary Mixtures of CO_2 and CH_4 in the Ionic Liquid 1-n-Butyl-3-methylimidazolium bis(trifluoromethylsulfonyl)imide. *Ind. Eng. Chem. Res.* **2015**, *54*, 8821-8828.

(57) Turner, C. H.; Cooper, A.; Zhang, Z.; Shannon, M. S.; Bara, J. E. Molecular simulation of the thermophysical properties of N-functionalized alkylimidazoles. *J. Phys. Chem. B* **2012**, *116*, 6529-6535.

(58) Martinez, L.; Andrade, R.; Birgin, E. G.; Martinez, J. M. PACKMOL: a package for building initial configurations for molecular dynamics simulations. *J. Comput. Chem.* **2009**, *30*, 2157-2164.

(59) Theodorou, D. N.; Suter, U. W. Detailed Molecular-Structure of a Vinyl Polymer Glass. *Macromolecules* **1985**, *18*, 1467-1478.

(60) Van Der Spoel, D.; Lindahl, E.; Hess, B.; Groenhof, G.; Mark, A. E.; Berendsen, H. J. GROMACS: fast, flexible, and free. *J. Comput. Chem.* **2005**, *26*, 1701-1718.

(61) Essmann, U.; Perera, L.; Berkowitz, M. L.; Darden, T.; Lee, H.; Pedersen, L. G. A smooth particle mesh Ewald method. *J. Chem. Phys.* **1995**, *103*, 8577-8593.

(62) Hoover, W. G. Canonical dynamics: Equilibrium phase-space distributions. *Phys. Rev. A* **1985**, *31*, 1695-1697.

(63) Parrinello, M.; Rahman, A. Crystal Structure and Pair Potentials: A Molecular-Dynamics Study. *Phys. Rev. Lett.* **1980**, *45*, 1196-1199.

(64) Shah, J. K.; Maginn, E. J. A general and efficient Monte Carlo method for sampling intramolecular degrees of freedom of branched and cyclic molecules. *J. Chem. Phys.* **2011**, *135*, 134121-134111.

(65) Shah, J. K.; Marin-Rimoldi, E.; Mullen, R. G.; Keene, B. P.; Khan, S.; Paluch, A. S.; Rai, N.; Romanielo, L. L.; Rosch, T. W.; Yoo, B.; Maginn, E. J. Cassandra: An open source Monte Carlo package for molecular simulation. *J. Comput. Chem.* **2017**, *38*, 1727-1739.

(66) Gelb, L. D.; Gubbins, K. E. Pore size distributions in porous glasses: A computer simulation study. *Langmuir* **1999**, *15*, 305-308.

(67) Kupgan, G.; Liyana-Arachchi, T. P.; Colina, C. M. Pore size tuning of poly(styrene-co-vinylbenzyl chloride-co-divinylbenzene) hypercrosslinked polymers: Insights from molecular simulations. *Polymer* **2016**, *99*, 173-184.

(68) Sarkisov, L.; Harrison, A. Computational structure characterisation tools in application to ordered and disordered porous materials. *Mol. Simulat.* **2011**, *37*, 1248-1257.

(69) Madkour, T. M.; Mark, J. E. Molecular modeling investigation of the fundamental structural parameters of polymers of intrinsic microporosity for the design of tailor-made ultra-permeable and highly selective gas separation membranes. *J. Membrane Sci.* **2013**, *431*, 37-46.

(70) Del Regno, A.; Gonciaruk, A.; Leay, L.; Carta, M.; Croad, M.; Malpass-Evans, R.; McKeown, N. B.; Siperstein, F. R. Polymers of Intrinsic Microporosity Containing Tröger Base for CO_2 Capture. *Ind. Eng. Chem. Res.* **2013**, *52*, 16939-16950.

(71) Wood, C. D.; Tan, B.; Trewin, A.; Su, F.; Rosseinsky, M. J.; Bradshaw, D.; Sun, Y.; Zhou, L.; Cooper, A. I. Microporous Organic Polymers for Methane Storage. *Adv. Mater.* **2008**, *20*, 1916-1921.

(72) Wood, C. D.; Tan, B.; Trewin, A.; Niu, H. J.; Bradshaw, D.; Rosseinsky, M. J.; Khimyak, Y. Z.; Campbell, N. L.; Kirk, R.; Stockel, E.; Cooper, A. I. Hydrogen storage in microporous hypercrosslinked organic polymer networks. *Chem. Mater.* **2007**, *19*, 2034-2048.

(73) Bisoi, S.; Mandal, A. K.; Padmanabhan, V.; Banerjee, S. Aromatic polyamides containing trityl substituted triphenylamine: Gas transport properties and molecular dynamics simulations. *J. Membrane Sci.* **2017**, *522*, 77-90.

(74) Espeso, J.; Lozano, A. E.; de la Campa, J. G.; de Abajo, J. Effect of substituents on the permeation properties of polyamide membranes. *J. Membrane Sci.* **2006**, *280*, 659-665.

(75) Zhuang, Y.; Seong, J. G.; Do, Y. S.; Jo, H. J.; Lee, M. J.; Wang, G.; Guiver, M. D.; Lee, Y. M. Effect of Isomerism on Molecular Packing and Gas Transport Properties of Poly(benzoxazole-co-imide)s. *Macromolecules* **2014**, *47*, 7947-7957.

(76) Weng, C.-J.; Jhuo, Y.-S.; Huang, K.-Y.; Feng, C.-F.; Yeh, J.-M.; Wei, Y.; Tsai, M.-H. Mechanically and Thermally Enhanced Intrinsically Dopable Polyimide Membrane with Advanced Gas Separation Capabilities. *Macromolecules* **2011**, *44*, 6067-6076.